NANO LETTERS

pubs.acs.org/NanoLett

Letter

Photodriven Catalytic Hydrogenation of CO_2 to CH_4 with Nearly 100% Selectivity over Ag_{25} Clusters

Yan Xiong, Hongwei Chen, Yi Hu, Songyuan Yang, Xiaolan Xue, Lingfeng He, Xu Liu,* Jing Ma,* and Zhong Jin*

Cite This: *Nano Lett.* 2021, 21, 8693−8700

Read Online

ACCESS | Metrics & More | Article Recommendations | Supporting Information

ABSTRACT: The conversion of chemically inert carbon dioxide and its photoreduction to value-added products have attracted enormous attention as an intriguing prospect for utilizing the principal greenhouse gas CO_2. Herein, we explore the use of Ag_{25} clusters with well-defined atomic structures for high-selectivity photocatalytic hydrogenation of CO_2 to methane. Ag_{25} clusters, with molecular-like properties and surface plasmon resonance, exhibit competitive catalytic activity for light-driven CO_2 reduction that yield an almost 100% product selectivity of methane at a relatively mild temperature (100 °C). DFT calculations reveal that the absorption of CO_2 on Ag_{25} clusters is energetically favorable. The methanation of the Ag_{25} cluster catalyst has been investigated by *operando* infrared spectroscopy, verifying that methane was produced through a −H-assisted multielectron reaction pathway via the transformation of formyl and formaldehyde species to form surface CH_x. This work presents a highly efficient strategy for high-performance CO_2 methanation via well-defined metal cluster catalysts.

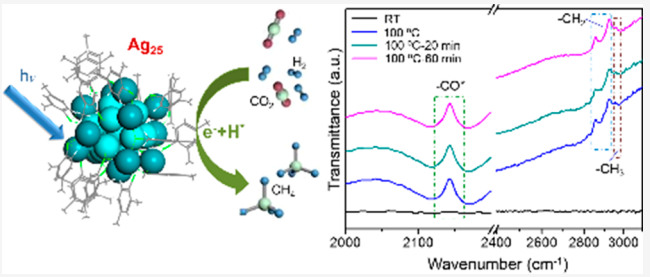

KEYWORDS: *Ag_{25} Clusters, CO_2 Hydrogenation, Photodriven catalysis, Operando IR*

INTRODUCTION

Conversion of CO_2 into hydrocarbons for the chemical industry is a promising approach to utilize renewable energy. As a feasible route, the photocatalytic reduction of CO_2 to value-added products, such as CH_3OH and CH_4, has been actively investigated.[1,2] Particularly, the thermodynamically favorable CO_2 reduction to methane ($\Delta G_{298} = -130.8$ kJ/mol) is a highly desirable process, because methane as a value-added C_1 product has widespread applications (fuel and chemical raw materials).[3,4] In previous studies, CO_2 hydrogenation toward CH_4 has mainly been based on heterogeneous catalysis of group VIII metals (e.g., Fe, Co, Ru, and Rh) loaded on transition-metal oxides (such as SiO_2, TiO_2, and Al_2O_3). However, the selectivity or efficiency is not satisfactory (Table S1),[5−8] and also the CO_2 hydrogenation reaction systems usually require strict experimental conditions, such as high pressure and high temperature. To promote the CO_2 conversion under mild conditions, photoreduction of CO_2 via transition-metal catalysts (such as Au, Cu, and Ag) that possess distinct optical and electronic properties has garnered much interest due to localized surface plasmon resonance (LSPR) of these metals in the UV−vis region.[9−14] The LSPR effect that can promote catalytic performance by broadening the light response range and enhancing photogenerated charge carrier separation through local field enhancement or hot electron injection. Moreover, the exploration of molecular homogeneous catalytic systems for CO_2 conversion has also attracted widespread attention, as these molecular complexes can act as both photo- and electrocatalysts.[15,16]

In previous studies, metal clusters with protected ligands have exhibited great potential in catalysis. They can link the size gap between molecules and large nanoparticles and also possess unique electronic and catalytic properties, which differ from those of large nanoparticles and bulk metal surfaces in catalytic reactions.[17,18] Au_{25}, Au_{24}, Au_{21}, and Cu_4 clusters with narrow size distributions have been successfully synthesized, and these materials have shown remarkable performances in catalytic reactions.[17−22] Herein, we report Ag_{25} clusters for a highly efficient photodriven CO_2 reduction reaction (CO_2RR) to CH_4 with nearly 100% selectivity under relatively mild conditions (100 °C), attributed to the competitive catalytic activity and LSPR effect of Ag_{25} clusters.[23,24] *Operando* infrared (IR) spectroscopy and density functional theory (DFT) calculations show that Ag_{25} clusters can efficiently facilitate CO_2 methanation via an energetically favorable multielectron pathway. This study indicates that metal clusters with precise atomic structures can serve as promising catalysts for

Received: July 18, 2021
Revised: August 29, 2021
Published: October 5, 2021

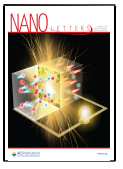

https://doi.org/10.1021/acs.nanolett.1c02784
Nano Lett. 2021, 21, 8693−8700

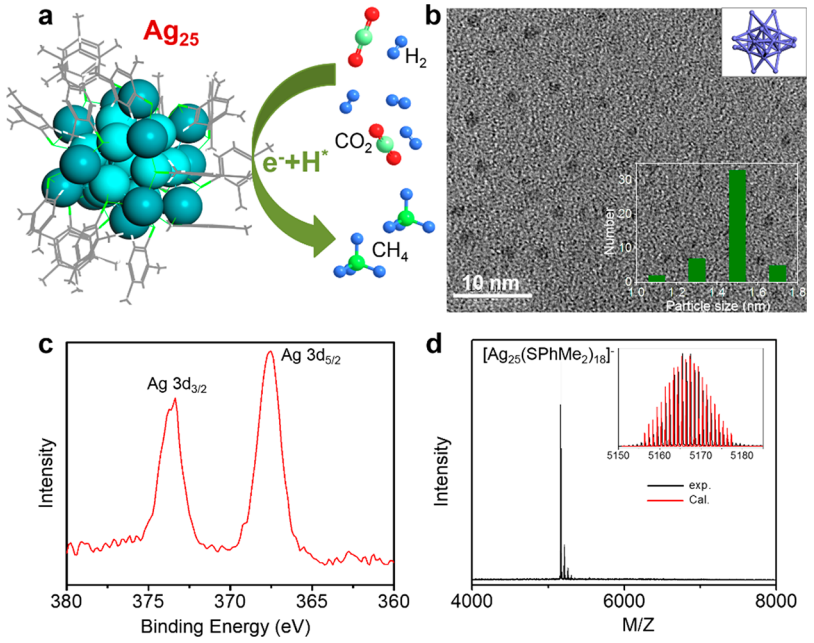

Figure 1. Morphology and composition characterizations of Ag_{25} clusters. (a) Schematic model of a Ag_{25} cluster for CO_2 photoreduction. (b) HRTEM image of Ag_{25} clusters. The inset shows the structural framework of the Ag_{25} cluster. (c) Ag 3d XPS spectrum of Ag_{25} clusters. (d) Positive-ion reflectron electrospray ionization mass spectrum (ESI-MS) of Ag_{25} clusters.

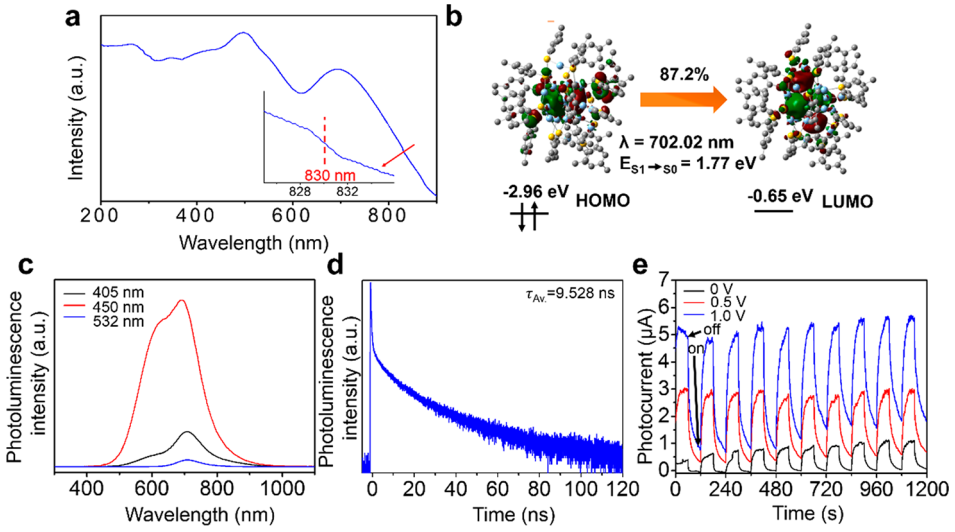

Figure 2. Photoelectric characterizations. (a) UV−vis absorption spectrum of Ag_{25} clusters. The inset shows an absorption shoulder at 830 nm. (b) Isosurface plot of the frontier orbitals of the crystal structure of the Ag_{25} cluster. (c) Steady-state PL spectra at different excitation wavelengths. (d) Time-resolved transient PL decay spectrum with an excitation wavelength of 450 nm. (e) Time-dependent photocurrent spectra of Ag_{25} clusters at different bias voltages of 0, 0.5, and 1.0 V with the lights on and off.

photodriven CO_2 fixation and also can be investigated to better understand the property differences from the molecular aggregates of metal atoms to the bulk metals.

RESULTS AND DISCUSSION

Structural Analyses. The Ag_{25} clusters were atomically precise without fragmentation and were obtained via a kinetically controlled synthetic method. The cluster has an incomplete shell (12 silver atoms) in six extended staples (−S−Ag−S−Ag−S-Ag−) that encompass a Ag_{13} icosahedral core (abbreviated as Ag_{25}), which exhibits a fascinating atom-packing structure and catalytic performance. The special atomic structure enables catalysis to occur on all core and surface atoms, which is totally completely different from the case of bulk materials. Particularly, each atom in Ag_{25} clusters might act as a catalyst.[25] A schematic illustration of a Ag_{25} cluster for photoinduced CO_2 hydrogenation is postulated in Figure 1a, showing the multielectron reaction pathway toward the formation of CH_4.

The morphology of Ag_{25} clusters was investigated by high-resolution transmission electron microscopy (HRTEM) (Figure 1b). It can be observed that ultrafine and homogeneously distributed Ag_{25} clusters with minimal aggregation were formed, and the core diameter of the prepared Ag_{25} clusters was approximately 1.5 nm. The inset in Figure 1b shows the simplified atomic structure of Ag_{25}, with

https://doi.org/10.1021/acs.nanolett.1c02784
Nano Lett. 2021, 21, 8693−8700

an Ag_{13} core enclosed by six Ag_2S_3 semiring structures as a shell (note that thiolate is omitted for clarity). The chemical status and Ag^0 content of Ag_{25} clusters were further examined by X-ray photoelectron spectroscopy (XPS). Two peaks of Ag 3d spectra of Ag_{25} clusters (367.9 and 373.8 eV, Figure 1c) are ascribed to the binding energies of Ag $3d_{5/2}$ and Ag $3d_{3/2}$, respectively, in compliance with a zerovalent state (Ag $3d_{5/2} \approx$ 368.0 eV) for Ag atoms. Electrospray ionization mass spectrometry (ESI-MS), which is an invaluable tool to reveal metal nanoclusters, has been applied to analyze Ag_{25} clusters. As shown in Figure 1d, a distinct peak at 5142 Da hints that the ionized clusters carry a +1 charge, which corresponds to the chemical formula $Ag_{25}(SPhMe_2)_{18}$. The other observed peaks are derived from the molecular fragments that could be due to the loss of L_2, Ag_2L_2, Ag_3L_3, Ag_4L_4, and Ag_5L_5 species from the parent peak or to sequential loss of L/AgL units (where L = $SPhMe_2$).[26]

Photoelectric Properties. The light absorption spectrum and frontier orbitals of Ag_{25} clusters are presented in Figure 2a,b. An absorption feature attributed to the Ag_{25} clusters was revealed by the UV−vis spectrum (Figure 2a), which is consistent with previous studies.[25,27,28] The Ag_{25} clusters display four dominant absorption peaks at 346, 410, 496, and 693 nm, respectively, as well as a broad absorption shoulder band centered at 830 nm. The absorption shoulder identified that the energy gap between the highest occupied and lowest unoccupied molecular orbitals (HOMO and LUMO) of the Ag_{25} cluster is 1.48 eV.[29,30] The vertical excitation energies of the Ag_{25} cluster were studied by a time-dependent DFT (TDDFT) method; the calculated peaks at 600−700 nm are displayed in a histogram which are consistent with the UV spectrum obtained from experiment (Figure S1). The electron transition diagram of Ag_{25} at the lowest excitation was revealed by TDDFT calculations (Figure 2b), which verifies that the Ag_{25} cluster has a discrete molecular-like electronic structure.

The light absorption properties of Ag_{25} clusters are mainly featured by their molecular-like cluster structure. The multiband UV−vis absorption spectrum of Ag_{25} clusters is ascribed to their HOMO → LUMO and HOMO-1/2 → LUMO transitions (Figures S2−S4). Due to the nanometer-scale particle size, the Ag_{25} clusters show a discrete electronic structure, which is close to the reported results.[17,31] In the UV (ca. <400 nm) region, the Ag_{25} cluster absorption effect is dominated by LSPR properties induced by the interaction between the incident light and the surface of Ag_{25} clusters.[32,33]

The Ag_{25} cluster charge transfer capacity was studied via steady-state photoluminescence (PL), time-resolved transient PL decay spectra, and time-dependent photocurrent responses. The steady-state PL spectra were investigated independently at excitation wavelengths of 405, 450, and 532 nm, as shown in Figure 2c. The PL spectra did not exhibit significant position changes with an increase in excitation wavelength, and the locations of all emission peaks were nearly the same. The optimal excitation wavelength of Ag_{25} clusters is 450 nm. The average fluorescence lifetime obtained by time-resolved transient PL for Ag_{25} clusters is 9.528 ns (Figure 2d; the PicoQuant FluoFit data are shown in Table S2). The PL decay time of Ag_{25} clusters is longer than those of the transient metals or transition-metal dichalcogenides reported in the literature.[34−36] The longer PL lifetime indicates a retarded carrier recombination on the nanosecond time scale of Ag_{25} clusters, resulting in less dispersion in the decay rates and a reduction in nonradiative recombination. Ultimately, this will benefit the photocatalytic performance.[37,38]

The hot electrons generated via the LSPR effect can be evaluated through short-circuit photocurrents, which are measured under three independent applied bias voltages.[39] The Ag_{25} clusters were affixed to indium tin oxide (ITO) surfaces, and it was found that the photoexcitation of Ag_{25} clusters indeed led to the generation of a net photocurrent, as shown in Figure 2e. Excellent repetition of the photocurrent originating from the Ag_{25} clusters was observed under photoswitching conditions. A peak photocurrent of 5.7 μA was achieved at a bias of 1.0 V. However, the current intensity decays with light turned off. This phenomenon agrees well with the time-resolved transient PL result and demonstrates that the Ag_{25} clusters undergo long-time retarded carrier recombination. The intensity of the photocurrent was relatively low due to a rapid thermalization of the generated charge carriers in the metal.

Photodriven Catalytic Performances. Ag_{25} clusters can serve a dual role in the photodriven reaction of CO_2, offering light absorption and catalytic sites to activate the absorbed CO_2. To verify this assumption, photodriven catalytic CO_2 reduction was performed on Ag_{25} clusters supported on a Whatman GF/F glass microfiber membrane under a 300 W Xe lamp illumination (VisREF 350−780 nm) without or with a cutoff filter (420 nm), as detailed in the Experimental Section in the Supporting Information. Before the catalytic reaction, the temperature of the catalyst bed was measured by a Fotric 225 thermal camera at varying heights (i.e., the vertical distance from catalyst bed to lamp), as shown in Figure S5. It confirmed that the catalyst bed temperature could be raised by ∼80 °C under 300 W Xe lamp at the reaction height (15 cm, as shown in Figure S5a and b).

For further comparison, Ag NPs (∼20 nm average diameter) were also used as a control sample. Figure 3a shows the CO_2 photoreduction activity of Ag_{25} clusters and Ag NP catalysts under different conditions (without any applied potential). The CO_2 reduction promoted by Ag_{25} clusters yielded the hydrocarbon product methane, with 28.95 μmol h^{-1} mg^{-1} productivity at 100 °C and Xe lamp illumination without a cutoff filter, which can compete with the state of the art metal cluster catalysts (such as Au and Cu clusters) (Table S1). The signal of CO or other gas/liquid products was not detected or was below the detection limits, indicating that these are not produced or were under the GC (40 ppm) or ^{1}H NMR detection limit (10 ppm) (Figure S6). CO as the primary product for electrocatalytic reduction of CO_2 on Ag due to its weak binding prevents its further reduction.[40] However, with the LSPR-induced surface charge-carrier-rich Ag_{25} clusters, the CO_2RR process is completely changed in comparison with the electrocatalytic CO_2 reduction process that transferred to a multielectron system with high hydrocarbon selectivity. Moreover, the catalytic performance of Ag_{25} clusters was investigated under light irradiation with a 420 nm cutoff filter. Again, CH_4 was the only hydrocarbon product (25.34 μmol h^{-1} mg^{-1}). The gradual decrease in methane productivity is most likely due to the light source below 420 nm not being utilized. When the incident light intensity was varied from 100 to 360 mW cm^{-2}, the photothermal catalytic performance of the Ag_{25} clusters did not show an obvious change (Figure S7a). As a comparison, Ag NPs were used for the CO_2 photoreduction under the same conditions as for Ag_{25}, and there was

https://doi.org/10.1021/acs.nanolett.1c02784
Nano Lett. 2021, 21, 8693−8700

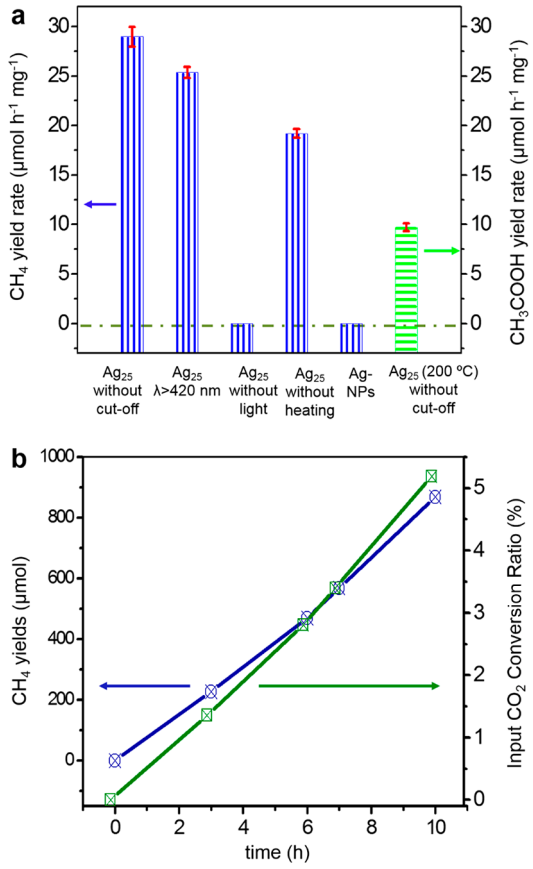

Figure 3. Photodriven CO_2 conversion measurements. (a) CH_4 and CH_3COOH yields via photodriven catalytic reduction of CO_2 over Ag_{25} clusters. Reaction conditions: CO_2 and H_2 (1:3 in volume, 1.5 MPa). (b) Variations in CH_4 productivity and CO_2 conversion efficiency with different reaction times.

no catalytic performance for the Ag NPs at 100 °C, as shown in Figure 3a.

Without light illumination, the hydrocarbon outcome was not detectable under dark conditions at 100 °C (Figure S8). In other words, the synergistic catalysis effect of the excitation light and the photodriven effect, rather than only external heating, is of critical importance for driving the photocatalytic CO_2 hydrogenation reaction.[41] When the Ag_{25} catalyst was tested with only light illumination (without assistant heating), the CH_4 generation rate greatly decreased to 19.18 μmol h^{-1} mg^{-1}. The lower C_1 evolution rate without assistant heating may be caused by the slower movement of generated electrons. This suggests that the movement of electrons can be significantly promoted by the heat, while the recombination of photoinduced electrons and holes is not increased, as confirmed in previous literature.[42,43] Another control experiment was conducted by increasing the reaction temperature to 200 °C for photodriven catalytic CO_2 with Ag_{25} clusters. The hydrogenation product was changed from CH_4 to CH_3COOH with a productivity of 9.71 μmol h^{-1} mg^{-1} at a 200 °C reaction temperature. Other liquid/gas products, such as CO, methanol, and ethanol, were not detected or were below the detection limit of the ^1H NMR (10 ppm) and GC (40 ppm) (Figure S9). In order to study the transition of photodriven products from CH_4 to CH_3COOH on Ag_{25} clusters, two other reaction temperatures (140 and 170 °C) were also investigated. As shown in Figure S7b, when the temperature was increased to 140 °C, the yield of CH_4 showed a slight decrease in comparison to that at 100 °C. When the temperature was increased to 170 °C, the CH_4 yield rate decreased to 7.12 μmol h^{-1} mg^{-1} and acetic acid was obtained with a yield rate of 4.11 μmol h^{-1} mg^{-1}. We suggest that the switch of the main product from CH_4 to CH_3COOH can be ascribed to the change in the dominant reaction pathway at different temperatures. In this work, the dominant reaction pathway of the CO_2 hydrogenation process totally changed at higher reaction temperatures. At 200 °C, the −CO reaction intermediate may exist, which will be bonded to Ag−CH_3 species and then produce acetic acid, as confirmed in previous literature.[44] Another possible reaction route for the production of acetic acid may be ascribed to the reaction of CH_4 and H_2O molecules at high temperatures through the following conversion pathway:[45]

$$2CH_4 + 2H_2O \rightarrow CH_3COOH + 8H^+ + 8e^- \quad (1)$$

The time factor of the input CO_2 conversion was also investigated (Figure 3b). The productivity of CH_4 in the reactor gradually increases from 227.38 μmol at 3 h to 868.5 μmol at 10 h, which means that the photoreduction of CO_2 continues to occur over time. As revealed in Figure 3b, the conversion ratio of CO_2 in the reactor enhanced by photoirradiation reached 1.38% after the first 3 h of the reaction and then reached 5.19% after 10 h of reaction. This is ascribed to the continuous conversion of light and thermal energy to chemical energy over time, and the reaction is far from equilibrium during photocatalytic CO_2 reduction. Meanwhile, the chemical composition, optical absorption spectrum, and morphology stability of Ag_{25} clusters after the photothermal test at 100 °C were investigated by ESI-MS, UV−vis, and HRTEM measurements, respectively (Figure S10). The unchanged chemical compositions demonstrated that sulfur ligands were not oxidized during the long-term reaction at 100 °C, and the unchanged light absorption spectrum and excellent morphology stability verified that the particle size and surface dispersibility of Ag_{25} clusters were well maintained under the reaction conditions of 100 °C without aggregation. The chemical composition of the Ag_{25} clusters after a long-term reaction at a high temperature of 200 °C was also investigated by ESI-MS (Figure S10d). This revealed that the chemical composition is transformed at a high temperature of 200 °C, suggesting that the ligands had fallen off or the sulfur ligands might be oxidized on treatment at a high reaction temperature (200 °C). This result suggests that a mild reaction temperature (100 °C) is beneficial to the catalytic stability of Ag_{25} clusters for CO_2 to methane conversion.

Catalytic Reaction Pathway. As the major product of the CO_2RR catalyzed by Ag_{25} clusters is CH_4, we mainly considered and proposed the possible intermediates on the pathways toward CO_2 to CH_4 conversion on Ag_{25} clusters, as summarized and illustrated in Figure 4a. The hydrogen source dissociated from H_2 acts as a reactant on Ag_{25} clusters and plays a crucial role in the CO_2 reduction reaction. Theoretical studies suggest that the corner and edge atoms of silver are actually able to activate molecular hydrogen.[46] For Ag_{25} clusters, surface silver atoms with a low coordination property (coordination number 3) could afford a favorable circumstance for hydrogen adsorption and dissociation.[47,48] Hot electrons excited by the plasmon effect over Ag_{25} clusters were injected to dissociate the adsorbed hydrogen with an antibonding state.

https://doi.org/10.1021/acs.nanolett.1c02784
Nano Lett. 2021, 21, 8693−8700

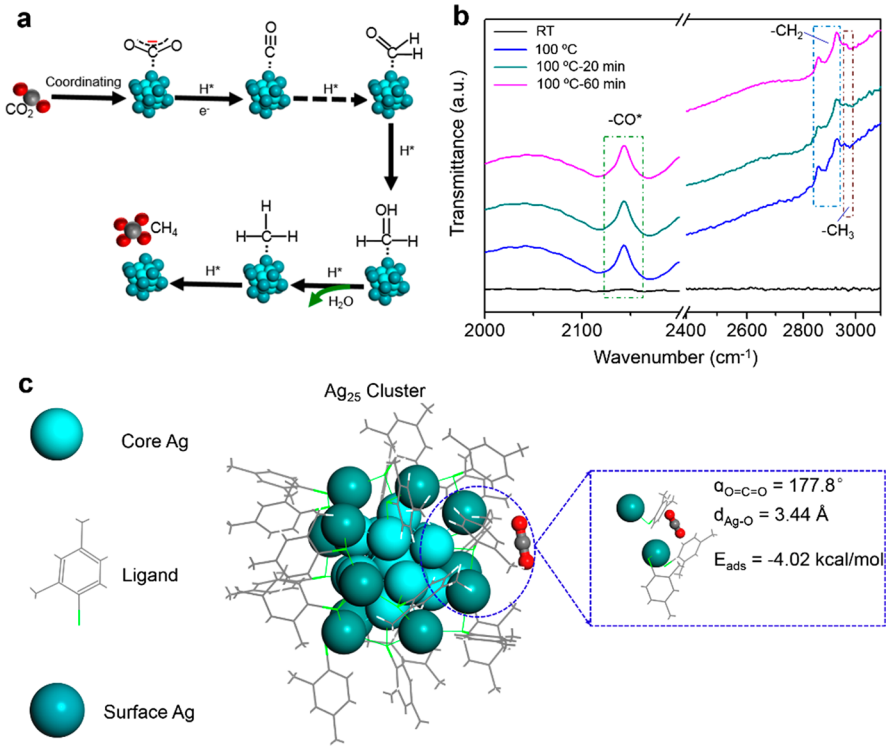

Figure 4. (a) Proposed reaction intermediates and pathway of CO_2 to CH_4 conversion on Ag_{25} clusters. (b) Time-resolved *operando* IR spectra of reaction intermediates on Ag_{25} clusters at 100 °C for CO_2 RR. Reaction conditions: CO_2 and H_2 (1:3 in volume, 1.5 MPa). (c) DFT-calculated binding performance of CO_2 on the Ag_{25} cluster.

The intermediates that were generated in CO_2RR system were investigated by time-resolved *operando* IR spectroscopy (Figure S11a). The band at 2142 cm^{-1} is assigned to CO* (Figure 4b), which is obtained via dissociation of carbon dioxide. The C−H stretching vibration can be assigned to surface formate (2924 cm^{-1}).[49] Meanwhile, the bands at 2854 and 2963 cm^{-1} are assigned to C−H vibrations of CH_2 and CH_3 species, respectively. This result indicates that $-CH_2OH$ species might be a further intermediate of formate hydrogenation. As a result, the reaction mechanism of CO_2 hydrogenation on Ag_{25} clusters is initially ascribed to an adsorbed CO_2 molecule being activated to a $*CO_2$ intermediate. Then, simultaneous multiple proton/electron transfer occurs during the reaction process, and CH_4 was generated via a −H-assisted process, probably by the transformation of formyl (HCO*) and formaldehyde (H_2CO*) species to form surface CH_x. In general, the specific packing structures and compositions of Ag_{25} clusters synergistically determine the reaction kinetics, formation free energies, and adsorption strengths of the reaction intermediates in the CO_2 hydrogenation, aiming at achieving highly effective selectivity and activity.

The binding behavior of CO_2 on the Ag_{25} cluster was studied by DFT calculations, as shown in Figure 4c. The angle of CO_2 changed from 180 to 177.8° after absorption on the Ag_{25} cluster. This suggests that the CO_2 molecule was activated after coordination to the Ag_{25} cluster. The binding energy of CO_2 absorbed on the Ag_{25} cluster is 4.02 kcal/mol, as estimated by DFT calculations, indicating that the CO_2 absorption on Ag_{25} clusters is energetically favorable (Figure 4c). The possible mechanism conception is $Ag_{25}(SPhMe_2)_{18}$ cluster with a discrete electronic state and incomplete Ag_{12} exterior shell which is benefit to the remarkable catalytic activity and selectivity. Meanwhile, the electron-rich silver core (Ag_{13}) is also conducive to the selective C = O bonds hydrogenation. Under light illumination, the LSPR effect induced hot electron will transfer on Ag_{25} clusters and carbon dioxide interface, contributing to C_1 product from reduced CO_2 and raised Fermi level (EF') at steady state. A higher EF' favors a rapidly hot electrons transferring to the adsorbed CO_2 molecules. The Ag_{25} clusters are cathodically polarized by plasmonic excitation which will induce abundant energetic electrons to activate carbon dioxide. The free CO_2 molecules adsorption onto the cluster surface slightly changed the electron hybridization state on Ag_{25} clusters (Figure S12). The hot electrons produced from plasmonic excitation are injected into the adsorbed carbon dioxide molecule that generates the $CO_2^{\bullet-}$ intermediate (or hydrogenated species). Therewith, unsaturated aldehyde intermediates (such as −CHO) was obtained through an activated C═O group attacked by nucleophilic hydrogen. However, this one-electron transfer is assumed to be the rate-determining step (RDS) on account of a huge energy consumption (~1.9 eV) to acquire $CO_2^{\bullet-}$ to activate the inert CO_2 molecule.[50] When this RDS process is broken through, methane can be easily obtained though a multielectron cascade catalytic process with the acquired $CO_2^{\bullet-}$ (or hydrogenated species).

CONCLUSION

In summary, the photodriven CO_2 reduction over Ag_{25} clusters exhibits high activity and superior CH_4 selectivity. The molecular-like structure and plasmonic properties of Ag_{25} clusters allow it to interact better with CO_2, thus benefiting its multielectron photocatalytic conversion. The strong interaction of light with matter over plasmonic clusters renders extraordinary attributes: (1) allowing to drive kinetically

https://doi.org/10.1021/acs.nanolett.1c02784
Nano Lett. 2021, 21, 8693−8700

challenging multielectron reactions by light illumination and (2) enabling the control of the catalytic reaction and selectivity through a suitable option of light excitation properties. This work affords a deep understanding of photoelectronic properties and catalysis mechanism involved in Ag_{25} clusters. We hope it may stimulate further studies toward developing more efficient light-responsive metal clusters with well-defined atomic structures for CO_2 conversion by utilizing clean solar energy.

■ ASSOCIATED CONTENT

Supporting Information

. Figures S1−S13 and Table S1−S2; (PDF) The Supporting Information is available free of charge at https://pubs.acs.org/doi/10.1021/acs.nanolett.1c02784.

Synthetic details, experimental section, computational methods, calculated absorption spectra, ^{1}H NMR and GC spectra for all reactions, ESI-MS spectra, HRTEM images, UV−vis spectrum, photographs of the experimental setup, and the standard calibration curve for acetic acid (PDF)

■ AUTHOR INFORMATION

Corresponding Authors

Xu Liu − *MOE Key Laboratory of Mesoscopic Chemistry, MOE Key Laboratory of High Performance Polymer Materials and Technology, Jiangsu Key Laboratory of Advanced Organic Materials, School of Chemistry and Chemical Engineering, Nanjing University, Nanjing 210023, People's Republic of China;* orcid.org/0000-0003-0668-5074; Email: xuliu@nju.edu.cn

Jing Ma − *MOE Key Laboratory of Mesoscopic Chemistry, MOE Key Laboratory of High Performance Polymer Materials and Technology, Jiangsu Key Laboratory of Advanced Organic Materials, School of Chemistry and Chemical Engineering, Nanjing University, Nanjing 210023, People's Republic of China;* orcid.org/0000-0001-5848-9775; Email: jingma@nju.edu.cn

Zhong Jin − *MOE Key Laboratory of Mesoscopic Chemistry, MOE Key Laboratory of High Performance Polymer Materials and Technology, Jiangsu Key Laboratory of Advanced Organic Materials, School of Chemistry and Chemical Engineering, Nanjing University, Nanjing 210023, People's Republic of China; Shenzhen Research Institute of Nanjing University, Shenzhen 518063, People's Republic of China;* orcid.org/0000-0001-8860-8579; Email: zhongjin@nju.edu.cn

Authors

Yan Xiong − *MOE Key Laboratory of Mesoscopic Chemistry, MOE Key Laboratory of High Performance Polymer Materials and Technology, Jiangsu Key Laboratory of Advanced Organic Materials, School of Chemistry and Chemical Engineering, Nanjing University, Nanjing 210023, People's Republic of China*

Hongwei Chen − *MOE Key Laboratory of Mesoscopic Chemistry, MOE Key Laboratory of High Performance Polymer Materials and Technology, Jiangsu Key Laboratory of Advanced Organic Materials, School of Chemistry and Chemical Engineering, Nanjing University, Nanjing 210023, People's Republic of China*

Yi Hu − *MOE Key Laboratory of Mesoscopic Chemistry, MOE Key Laboratory of High Performance Polymer Materials and Technology, Jiangsu Key Laboratory of Advanced Organic Materials, School of Chemistry and Chemical Engineering, Nanjing University, Nanjing 210023, People's Republic of China*

Songyuan Yang − *MOE Key Laboratory of Mesoscopic Chemistry, MOE Key Laboratory of High Performance Polymer Materials and Technology, Jiangsu Key Laboratory of Advanced Organic Materials, School of Chemistry and Chemical Engineering, Nanjing University, Nanjing 210023, People's Republic of China*

Xiaolan Xue − *MOE Key Laboratory of Mesoscopic Chemistry, MOE Key Laboratory of High Performance Polymer Materials and Technology, Jiangsu Key Laboratory of Advanced Organic Materials, School of Chemistry and Chemical Engineering, Nanjing University, Nanjing 210023, People's Republic of China*

Lingfeng He − *MOE Key Laboratory of Mesoscopic Chemistry, MOE Key Laboratory of High Performance Polymer Materials and Technology, Jiangsu Key Laboratory of Advanced Organic Materials, School of Chemistry and Chemical Engineering, Nanjing University, Nanjing 210023, People's Republic of China*

Complete contact information is available at: https://pubs.acs.org/10.1021/acs.nanolett.1c02784

Author Contributions

Z.J. and Y.X. conceived the idea of this study and designed the experiments. X.L. performed Ag_{25} cluster synthesis. Y.X. performed photoelectric measurements, catalytic tests, and data analysis. H.C., L.H., and J.M. performed theoretical calculations. Y.X. and Y.H. performed the material characterizations. All of the authors analyzed the data and discussed the results. Y.X. and Z.J. cowrote and revised the manuscript. Z.J. supervised the project.

Notes

The authors declare no competing financial interest.

■ ACKNOWLEDGMENTS

This work was supported by the National Key Research and Development Program of China (2017YFA0208200), the Fundamental Research Funds for the Central Universities of China (0205-14380266), the National Natural Science Foundation of China (22022505, 21872069), the Natural Science Foundation of Jiangsu Province (BK20180008), and the Shenzhen Fundamental Research Program of Science, Technology and Innovation Commission of Shenzhen Municipality (JCYJ20180307155007589).

■ REFERENCES

(1) In, S.; Vaughn, D. D.; Schaak, R. E. Hybrid CuO-$TiO_{2-x}N_x$ hollow nanocubes for photocatalytic conversion of CO_2 into methane under solar irradiation. *Angew. Chem., Int. Ed.* **2012**, *51*, 3915−3918.

(2) Wang, W.-H.; Himeda, Y.; Muckerman, J. T.; Manbeck, G. F.; Fujita, E. CO_2 hydrogenation to formate and methanol as an alternative to photo- and electrochemical CO_2 reduction. *Chem. Rev.* **2015**, *115*, 12936−12973.

(3) Caballero, A.; Pérez, P. J. Methane as raw material in synthetic chemistry: the final frontier. *Chem. Soc. Rev.* **2013**, *42*, 8809−8820.

(4) Martin, N. M.; Velin, P.; Skoglundh, M.; Bauer, M.; Carlsson, P.-A. Catalytic hydrogenation of CO_2 to methane over supported Pd, Rh and Ni catalysts. *Catal. Sci. Technol.* **2017**, *7*, 1086−1094.

(5) Sharma, S.; Hu, Z.; Zhang, P.; McFarland, E. W.; Metiu, H. CO_2 methanation on Ru-doped ceria. *J. Catal.* **2011**, *278*, 297−309.
(6) Centi, G.; Quadrelli, E. A.; Perathoner, S. Catalysis for CO_2 conversion: a key technology for rapid introduction of renewable energy in the value chain of chemical industries. *Energy Environ. Sci.* **2013**, *6*, 1711−1731.
(7) Dai, X.; Sun, Y. Reduction of carbon dioxide on photoexcited nanoparticles of VIII group metals. *Nanoscale* **2019**, *11*, 16723−16732.
(8) Yan, B.; Wu, Q.; Cen, J.; Timoshenko, J.; Frenkel, A. I.; Su, D.; Chen, X.; Parise, J. B.; Stach, E.; Orlov, A.; Chen, J. G. Highly active subnanometer Rh clusters derived from Rh-doped $SrTiO_3$ forCO_2 reduction. *Appl. Catal., B* **2018**, *237*, 1003−1011.
(9) Hou, W.; Cronin, S. B. A review of surface plasmon resonance-enhanced photocatalysis. *Adv. Funct. Mater.* **2013**, *23*, 1612−1619.
(10) Kang, Q.; Wang, T.; Li, P.; Liu, L.; Chang, K.; Li, M.; Ye, J. Photocatalytic reduction of carbon dioxide by hydrous hydrazine over Au−Cu alloy nanoparticles supported on $SrTiO_3/TiO_2$ coaxial nanotube arrays. *Angew. Chem.* **2015**, *127*, 855−859.
(11) Yu, S.; Wilson, A. J.; Heo, J.; Jain, P. K. Plasmonic control of multi-electron transfer and C−C coupling in visible-light-driven CO_2 reduction on Au nanoparticles. *Nano Lett.* **2018**, *18*, 2189−2194.
(12) Kim, C.; Hyeon, S.; Lee, J.; Kim, W. D.; Lee, D. C.; Kim, J.; Lee, H. Energy-efficient CO_2 hydrogenation with fast response using photoexcitation of CO_2 adsorbed on metal catalysts. *Nat. Commun.* **2018**, *9*, 3027.
(13) Zhang, X.; Li, X.; Zhang, D.; Su, N. Q.; Yang, W.; Everitt, H. O.; Liu, J. Product selectivity in plasmonicphotocatalysis for carbon dioxide hydrogenation. *Nat. Commun.* **2017**, *8*, 14542.
(14) Baffou, G.; Cichos, F.; Quidant, R. Applications and challenges of thermoplasmonics. *Nat. Mater.* **2020**, *19*, 946−958.
(15) Ishitani, O.; George, M. W.; Ibusuki, T.; Johnson, F. P. A.; Koike, K.; Nozaki, K.; Pac, C.; Turner, J. J.; Westwell, J. R. Photophysical behavior of a new CO_2 reduction catalyst, Re$(CO)_2$(bpy)$\{P(OEt)_3\}^{2+}$. *Inorg. Chem.* **1994**, *33*, 4712−4717.
(16) Rakowski Dubois, M.; Dubois, D. L. Development of molecular electrocatalysts for CO_2 reduction and H_2 production/oxidation. *Acc. Chem. Res.* **2009**, *42*, 1974−1982.
(17) Kauffman, D. R.; Alfonso, D.; Matranga, C.; Qian, H.; Jin, R. Experimental and computational investigation of Au_{25} clusters and CO_2: a unique interaction and enhanced electrocatalytic activity. *J. Am. Chem. Soc.* **2012**, *134*, 10237−10243.
(18) Liu, C.; Yang, B.; Tyo, E.; Seifert, S.; DeBartolo, J.; von Issendorff, B.; Zapol, P.; Vajda, S.; Curtiss, L. A. Carbon dioxide conversion to methanol over size-selected Cu_4 clusters at low pressures. *J. Am. Chem. Soc.* **2015**, *137*, 8676−8679.
(19) Alfonso, D. R.; Kauffman, D.; Matranga, C. Active sites of ligand-protected Au_{25} nanoparticle catalysts for CO_2 electroreduction to CO. *J. Chem. Phys.* **2016**, *144*, 184705.
(20) Austin, N.; Zhao, S.; McKone, J. R.; Jin, R.; Mpourmpakis, G. Elucidating the active sites for CO_2 electroreduction on ligand-protected Au_{25} nanoclusters. *Catal. Sci. Technol.* **2018**, *8*, 3795−3805.
(21) Cai, X.; Saranya, G.; Shen, K.; Chen, M.; Si, R.; Ding, W.; Zhu, Y. Reversible switching of catalytic activity by shuttling an atom into and out of gold nanoclusters. *Angew. Chem., Int. Ed.* **2019**, *58*, 9964−9968.
(22) Li, Q.; Russell, J. C.; Luo, T.-Y.; Roy, X.; Rosi, N. L.; Zhu, Y.; Jin, R. Modulating the hierarchical fibrous assembly of Au nanoparticles with atomic precision. *Nat. Commun.* **2018**, *9*, 3871.
(23) Sastre, F.; Versluis, C.; Meulendijks, N.; Rodriguez-Fernandez, J.; Sweelssen, J.; Elen, K.; Van Bael, M. K.; den Hartog, T.; Verheijen, M. A.; Buskens, P. Sunlight-fueled, low-temperature Ru-catalyzed conversion of CO_2 and H_2 to CH_4 with a high photon-to-methane efficiency. *ACS Omega* **2019**, *4* (4), 7369−7377.
(24) Grote, R.; Habets, R.; Rohlfs, J.; Sastre, F.; Meulendijks, N.; Xu, M.; Verheijen, M. A.; Elen, K.; Hardy, A.; Van Bael, M. K.; Hartog, T.; Buskens, P. Collective photothermal effect of Al_2O_3-supported spheroidal plasmonic Ru nanoparticle catalysts in the sunlight-powered Sabatier reaction. *ChemCatChem* **2020**, *12*, 5618−5622.
(25) Liu, Y.; Chai, X.; Cai, X.; Chen, M.; Jin, R.; Ding, W.; Zhu, Y. Central doping of a foreign atom into the silver cluster for catalytic conversion of CO_2 toward C-C bond formation. *Angew. Chem., Int. Ed.* **2018**, *57*, 9775−9779.
(26) Yao, C.; Chen, J.; Li, M.-B.; Liu, L.; Yang, J.; Wu, Z. Adding two active silver atoms on Au_{25} nanoparticle. *Nano Lett.* **2015**, *15*, 1281−1287.
(27) Yan, J.; Su, H.; Yang, H.; Malola, S.; Lin, S.; Hakkinen, H.; Zheng, N. Total structure and electronic structure analysis of doped thiolated silver $[MAg_{24}(SR)_{18}]^{2-}$ (M = Pd, Pt) Clusters. *J. Am. Chem. Soc.* **2015**, *137*, 11880−11883.
(28) Bootharaju, M. S.; Joshi, C. P.; Parida, M. R.; Mohammed, O. F.; Bakr, O. M. Templated atom-precise galvanic synthesis and structure elucidation of a $[Ag_{24}Au(SR)_{18}]^-$ nanocluster. *Angew. Chem., Int. Ed.* **2016**, *55*, 922−926.
(29) Tlahuice-Flores, A. Optical properties of thiolate-protected $Ag_nAu_{25-n}(SCH_3)_{18}^-$ clusters. *J. Nanopart. Res.* **2013**, *15*, 1771.
(30) Zhu, M.; Qian, H.; Jin, R. Thiolate-protected Au_{20} clusters with a large energy gap of 2.1 eV. *J. Am. Chem. Soc.* **2009**, *131*, 7220−7221.
(31) Link, S.; Wang, Z. L.; El-Sayed, M. A. Alloy formation of gold-silver nanoparticles and the dependence of the plasmon absorption on their composition. *J. Phys. Chem. B* **1999**, *103*, 3529−3533.
(32) Pan, A.; Yang, Z.; Zheng, H.; Liu, F.; Zhu, Y.; Su, X.; Ding, Z. Changeable position of SPR peak of Ag nanoparticles embedded in mesoporous SiO_2 glass by annealing treatment. *Appl. Surf. Sci.* **2003**, *205*, 323−328.
(33) Buceta, D.; Pineiro, Y.; Vazquez-Vazquez, C.; Rivas, J.; Lopez-Quintela, M. Metallic clusters: theoretical background, properties and synthesis in microemulsions. *Catalysts* **2014**, *4*, 356−374.
(34) Varnavski, O.; Ispasoiu, R. G.; Balogh, L.; Tomalia, D.; Goodson, T. Ultrafast time-resolved photoluminescence from novel metal−dendrimer nanocomposites. *J. Chem. Phys.* **2001**, *114*, 1962−1965.
(35) Palummo, M.; Bernardi, M.; Grossman, J. C. Exciton radiative lifetimes in two-dimensional transition metal dichalcogenides. *Nano Lett.* **2015**, *15*, 2794−2800.
(36) Robert, C.; Lagarde, D.; Cadiz, F.; Wang, G.; Lassagne, B.; Amand, T.; Balocchi, A.; Renucci, P.; Tongay, S.; Urbaszek, B.; Marie, X. Exciton radiative lifetime in transition metal dichalcogenide monolayers. *Phys. Rev. B: Condens. Matter Mater. Phys.* **2016**, *93*, 205423.
(37) Wang, S.; Guan, B. Y.; Lou, X. W. D. Construction of $ZnIn_2S_4$-In_2O_3 hierarchical tubular heterostructures for efficient CO_2 photoreduction. *J. Am. Chem. Soc.* **2018**, *140*, 5037−5040.
(38) Xia, P.; Antonietti, M.; Zhu, B.; Heil, T.; Yu, J.; Cao, S. Designing defective crystalline carbon nitride to enable selective CO_2 photoreduction in the gas phase. *Adv. Funct. Mater.* **2019**, *29*, 1900093.
(39) Mock, J. J.; Barbic, M.; Smith, D. R.; Schultz, D. A.; Schultz, S. Shape effects in plasmon resonance of individual colloidal silver nanoparticles. *J. Chem. Phys.* **2002**, *116*, 6755−6759.
(40) Bagger, A.; Ju, W.; Varela, A. S.; Strasser, P.; Rossmeisl, J. Electrochemical CO_2 reduction: a classification problem. *ChemPhysChem* **2017**, *18*, 3266−3273.
(41) Zhou, L.; Swearer, D. F.; Zhang, C.; Robatjazi, H.; Zhao, H.; Henderson, L.; Dong, L.; Christopher, P.; Carter, E. A.; Nordlander, P.; Halas, N. J. Quantifying hot carrier and thermal contributions in plasmonicphotocatalysis. *Science* **2018**, *362*, 69−72.
(42) Okamoto, K.; Niki, I.; Scherer, A.; Narukawa, Y.; Mukai, T.; Kawakami, Y. Surface plasmon enhanced spontaneous emission rate of quantum wells probed by time-resolved photoluminescence spectroscopy. *Appl. Phys. Lett.* **2005**, *87*, 071102.
(43) Zhang, X.; Li, X.; Reish, M. E.; Zhang, D.; Su, N. Q.; Gutierrez, Y.; Moreno, F.; Yang, W.; Everitt, H. O.; Liu, J. Plasmon-enhanced catalysis: distinguishing thermal and nonthermal effects. *Nano Lett.* **2018**, *18*, 1714−1723.
(44) Shan, J.; Li, M.; Allard, L. F.; Lee, S.; Flytzani-Stephanopoulos, M. Mild oxidation of methane to methanol or acetic acid on supported isolated rhodium catalysts. *Nature* **2017**, *551*, 605−608.

https://doi.org/10.1021/acs.nanolett.1c02784
Nano Lett. 2021, 21, 8693−8700

(45) Periana, R.; Mironov, O.; Jones, C. J. Catalytic, oxidative condensation of CH_4 to CH_3COOH in one step via CH activation. *Science* **2003**, *301*, 814−818.
(46) Andrews, L. Matrix infrared spectra and density functional calculations of transition metal hydrides and dihydrogen complexes. *Chem. Soc. Rev.* **2004**, *33*, 123−132.
(47) Mohammad, A. B.; Hwa Lim, K.; Yudanov, I. V.; Neyman, K. M.; Rosch, N. A computational study of H_2 dissociation on silver surfaces: the effect of oxygen in the added row structure of Ag(110). *Phys. Chem. Chem. Phys.* **2007**, *9*, 1247−1254.
(48) Yan, L.; Ding, Z.; Song, P.; Wang, F.; Meng, S. Plasmon-induced dynamics of H_2 splitting on a silver atomic chain. *Appl. Phys. Lett.* **2015**, *107*, 083102.
(49) Yam, M. F.; Ch'ng, Y. S.; Tan, C. S.; Loh, Y. C.; Ahmad, M.; Zaini Asmawi, M. Vasorelaxation study and tri-step infrared spectroscopy analysis of Malaysian local herbs. *J. Pharmacopuncture.* **2016**, *19*, 145−154.
(50) Kumaravel, V.; Bartlett, J.; Pillai, S. C. Photoelectrochemical conversion of carbon dioxide (CO_2) into fuels and value-added products. *ACS Energy Lett.* **2020**, *5*, 486−519.

https://doi.org/10.1021/acs.nanolett.1c02784
Nano Lett. 2021, 21, 8693−8700